doi:10.1016/j.jmb.2008.03.029 J. Mol. Biol. (2008) 378, 828–839

JMB

Available online at www.sciencedirect.com

ScienceDirect

ELSEVIER

Salt-bridge Dynamics Control Substrate-induced Conformational Change in the Membrane Transporter GlpT

Christopher J. Law[1]†, Jonas Almqvist[2]*†, Adam Bernstein[1], Regina M. Goetz[1,2], Yafei Huang[3], Celine Soudant[1], Aatto Laaksonen[4], Sven Hovmöller[2] and Da-Neng Wang[1]*

[1]*The Helen L. and Martin S. Kimmel Center for Biology and Medicine at the Skirball Institute of Biomolecular Medicine, and Department of Cell Biology, New York University School of Medicine 540 First Avenue, New York, NY 10016, USA*

[2]*Division of Structural Chemistry, Arrhenius Laboratory, Stockholm University, S-10691 Stockholm, Sweden*

[3]*Department of Molecular Biology, Uppsala Biomedical Center, Swedish University of Agricultural Sciences, Box 590, S-753 24 Uppsala, Sweden*

[4]*Division of Physical Chemistry, Arrhenius Laboratory, Stockholm University, S-10691 Stockholm, Sweden*

Received 4 February 2008; received in revised form 5 March 2008; accepted 13 March 2008
Available online 19 March 2008

Edited by J. Bowie

Active transport of substrates across cytoplasmic membranes is of great physiological, medical and pharmaceutical importance. The glycerol-3-phosphate (G3P) transporter (GlpT) of the *E. coli* inner membrane is a secondary active antiporter from the ubiquitous major facilitator superfamily that couples the import of G3P to the efflux of inorganic phosphate (P_i) down its concentration gradient. Integrating information from a novel combination of structural, molecular dynamics simulations and biochemical studies, we identify the residues involved directly in binding of substrate to the inward-facing conformation of GlpT, thus defining the structural basis for the substrate-specificity of this transporter. The substrate binding mechanism involves protonation of a histidine residue at the binding site. Furthermore, our data suggest that the formation and breaking of inter- and intradomain salt bridges control the conformational change of the transporter that accompanies substrate translocation across the membrane. The mechanism we propose may be a paradigm for organophosphate:phosphate antiporters.

Keywords: antiporter; membrane transport; major facilitator superfamily; molecular dynamics simulations; secondary active transport

*Corresponding authors. E-mail addresses: jonasa@struc.su.se; wang@saturn.med.nyu.edu.

† C.J.L. and J.A. contributed equally to this work

Abbreviations used: G3P, *sn*-glycerol 3-phosphate; GlpT, G3P transporter; OPA, organophosphate/phosphate antiporter; G6PT, glucose 6-phosphate transporter; MFS, major facilitator superfamily.

Introduction

The *sn*-glycerol-3-phosphate (G3P) transporter (GlpT) from the *Escherichia coli* inner membrane couples the outward flow of internal inorganic phosphate (P_i) to the uptake of G3P into the cell.[1] G3P is an important intermediate in both glycolysis

and phospholipid biosynthesis, and it can act too as the sole energy source for bacterial growth.[2,3] Transporters homologous to GlpT are distributed throughout eubacteria,[4–7] as well as in eukaryotes, including plants[8] and humans.[9] These proteins form the organophosphate:phosphate antiporter (OPA) family,[10] that also includes UhpT, a close GlpT homologue from *E. coli*, and the human glucose-6-phosphate transporter (G6PT).[11] In turn, the OPA family belongs to the major facilitator superfamily (MFS), the largest and most diverse of the secondary active transporter families, with members that transport numerous substrates of physiological, medical and pharmaceutical significance.[10,12,13] Although a detailed molecular mechanism has been proposed for the *E. coli* MFS symporter LacY,[14,15] some fundamental questions pertaining to the molecular mechanism of substrate binding and transport by GlpT and other OPA proteins remain unanswered.

Like other MFS transporters, GlpT is believed to operate via a single-binding site, alternating-access mechanism.[16] This mechanism is believed to consist of three steps, namely substrate-binding, interconversion of the substrate-binding site, followed by substrate release to the other side of the membrane.[17] The three-dimensional crystal structure of GlpT, determined in our laboratory earlier, has provided valuable insight into the mechanics of substrate-binding and translocation.[17,18] The N- and C-terminal domains of the protein, each composed of six transmembrane α–helices, saddle the substrate-translocation pore, which contains the substrate-binding site at its inner end (Fig. 1). A rocker-switch type movement of the two domains relative to each other catalyzes substrate translocation across the membrane.[18,19] The energy required for such conformational change is provided by substrate binding forces,[20,21] as well as Brownian motion.[19] As the published structure of GlpT is of the molecule in the absence of substrate, in the inward-facing or C_i conformation (the substrate-binding site is exposed to the cytoplasm), information about the residues that form the substrate-binding site could only be inferred. Two conserved, positively-charged residues, arginine 45 (R45) and arginine 269 (R269), located at the inner end of the substrate-translocation pore, were suggested to form part of the substrate-binding site.[18] Although this agrees with previous genetic and biochemical studies on the homologous *E. coli* UhpT[22] and human G6PT transporters, in which mutation of R28 (equivalent to GlpT R45) in the latter to histidine or cysteine causes glycogen storage disease type 1b,[23,24] the direct involvement of R45 and R269 in substrate binding has not been shown biochemically in GlpT.

Additional residues must also be involved directly in defining substrate specificity to GlpT. Interestingly, in the crystal structure of GlpT, a molecule of the detergent β–dodecylmaltoside (DDM), used during purification of the protein, was observed within the substrate-translocation pore (Figs. 1a and b). The DDM depresses the side chain of a lysine residue (K80) and prevents it from protruding into the pore (Figs. 1b and c). Although the role of this residue in substrate binding to GlpT is unknown, previous work showed that mutation of the equivalent residue in UhpT (K82) to a cysteine caused the loss of transport activity.[25] It is plausible therefore, that K80 too may be involved in substrate binding to GlpT. Further clues to yet other positively-charged residues that form the substrate-binding site in GlpT can again be gleaned from biochemical and mutagenesis studies on UhpT.[25,26] It has been proposed that the protonation state of a conserved histidine residue (H168) modulates the affinity of UhpT to substrate.[26] While the equivalent of H168 in GlpT (H165) is found lining the substrate-translocation pathway,

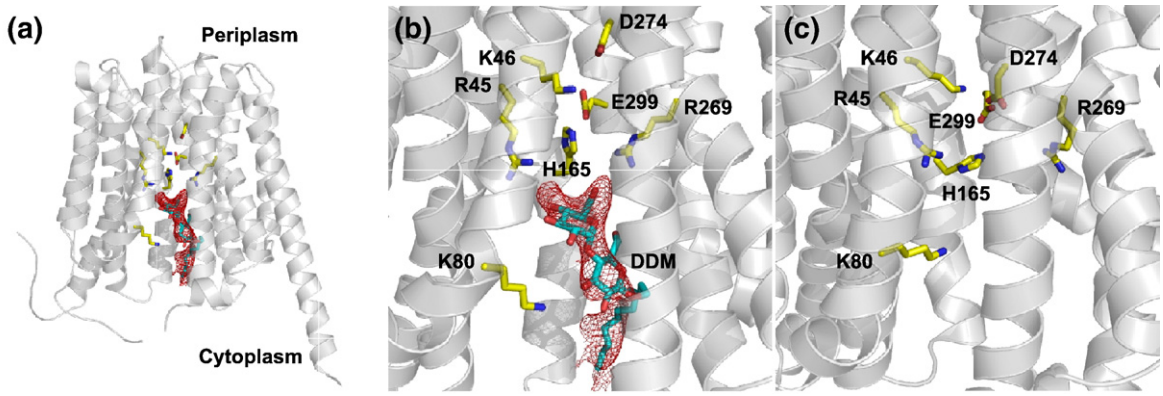

Fig. 1. The GlpT substrate-binding site. (a) the crystal structure of GlpT as viewed along the plane of the membrane, showing the position of the bound DDM molecule (represented by turquoise sticks along with F_o-F_c density contoured at 1.7 σ shown as red mesh). The residues proposed to be involved in substrate binding and salt bridge formation are depicted as yellow sticks; (b) the GlpT substrate-binding site in the 3.3 Å crystal-structure conformation consists of K80, R45, H165 and R269. In the crystal structure, a molecule of DDM depresses the K80 side chain preventing it from protruding into the substrate-translocation pore; (c) absence of DDM in MD simulations allows the K80 side chain to flip up into the substrate-translocation pore. The H165 and R269 residues changed conformation in the simulation compared to their conformation in the crystal structure. The coordinates for Fig. 3b were captured from the 20 ns time point of the simulation. Side chains are represented as yellow sticks and the transmembrane α–helices as grey ribbons.

making it amenable to interact with substrate, its role in substrate binding has not been investigated. Finally, several negatively-charged residues in the transmembrane regions are also conserved among OPA proteins, and mutations at the GlpT E299 and D274 equivalents in UhpT abolish transport.[25] Due to their negative charges, these residues cannot be directly involved in binding to anionic substrate; whether they participate in wider aspects of substrate translocation such as the triggering and control of conformational change during transport is unknown.

To understand the structural basis of substrate specificity, and the subsequent conformational change that leads to GlpT-catalyzed substrate translocation across the membrane, we investigated substrate binding to GlpT using a novel combination of molecular dynamics (MD) simulations, substrate-binding affinity assays in detergent solution, and transport activity assays in reconstituted proteoliposomes. This multifaceted approach has enabled us to forward both a detailed mechanism for substrate binding to GlpT and a novel scheme for the triggering and control of conformational changes

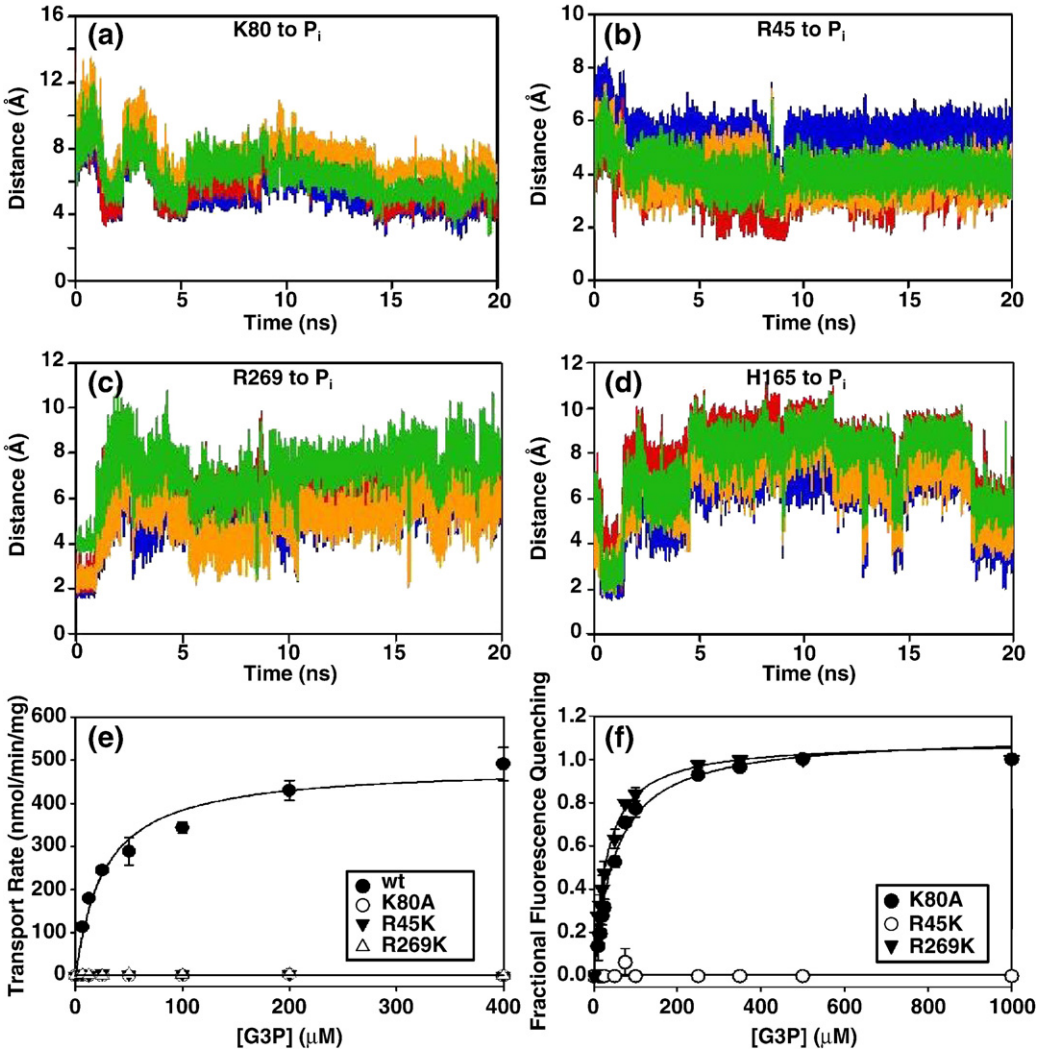

Fig. 2. Distances between the side chains of the key amino acid residues (K80, R45, R269 and H165) involved in substrate-binding to GlpT and the P_i substrate oxygens from molecular dynamics simulations on GlpT with P_i docked and H165 unprotonated (a–d), and the experimental measurements of the effect of mutating K80, R45 and R269 on transport activity and substrate-binding affinity (e and f). The distance from each side chain to the P_i oxygens is color-coded as follows: to O1, blue line; O2, red line; O3, orange line; and O4, green line. (a) distances between K80 and P_i substrate oxygens. K80 forms a stable interaction with P_i over the timescale of the simulation; (b) R45 interacts strongly with P_i when H165 is unprotonated, forming hydrogen bonds of 2–4 Å with three of the substrate oxygens; (c) the interactions between R269 and substrate oxygens are weak when H165 is unprotonated; (d) no stable interactions are established between unprotonated H165 and P_i substrate oxygens; (e) mutation of the K80, R45 and R269 residues abolishes transport activity of the mutant protein reconstituted into proteoliposomes. In contrast, the wt transporter displays saturation kinetics with a V_{max} of 487 nmol/min/mg and a K_m of 27 μM; (f) substrate-binding affinity of the K80A, R45K and R269K mutant transporters measured in detergent solution. The binding substrate-binding data for the wt transporter is omitted for clarity. The R45K mutant does not bind to G3P substrate. The K80A and R269K GlpT mutants retain the ability to bind to substrate, although much less tightly than wt GlpT, with apparent binding dissociation constants of 51 and 29 μM, respectively.

that occur during substrate translocation across the membrane.

Results and Discussion

K80, R45 and R269 are key determinants of substrate specificity for GlpT

In the GlpT crystal structure, a DDM molecule that co-crystallized with the protein depressed the K80 side chain (Fig. 1a). It is likely that in the absence of the detergent, as is the case with the transporter *in vivo*, the K80 side chain would project into the substrate-binding pore where it could interact with the oxygen moieties of the substrate molecule. This notion was supported by our MD simulations of the GlpT molecule in the C_i conformation, embedded in a palmitoyl-oleoyl-phosphatidylethanolamine (POPE) bilayer. In the absence of DDM, the positively charged K80 side chain in the simulated apoprotein structure was indeed found to flip up and extend into the substrate-binding pore where it could interact with substrate (Fig. 1b). The H165 residue also showed a large displacement from its crystal structure conformation (Fig. 1b). In contrast, both R45 and R269 displayed significantly less displacement.

To test for any interactions between the K80, R45 and R269 residues and substrate, and to identify substrate interactions with any other residues, we performed simulations with dibasic phosphate (P_i) docked to the equilibrated transporter in the C_i conformation. Although G3P also binds to the C_i conformation of GlpT, P_i was chosen for these simulations as it is the physiologically preferred substrate for the inward-facing conformation of the transporter. Our MD simulations supported the notion that R45 and R269 directly bind to substrates, as originally suggested by the GlpT crystal structure,[18] and that K80 too is part of the substrate-binding site. The substrate molecule was located closer to the N-terminal domain of the protein during the MD simulations, near the periplasmic end of the substrate translocation pore, and the three oxygen atoms in the P_i substrate were within 4 to 6 Å of the K80 side chain (Fig. 2a). R45, however, attracted the P_i substrate even stronger, with contacts between 2 to 4 Å established (Fig. 2b). In addition, the R45 side chain also maintained a highly stable ~2 Å salt bridge to D274. For R269, larger fluctuations occurred in the contacts with the P_i substrate during the simulation. After initial hydrogen bonding of 2 to 3 Å with the P_i oxygens, these bonds quickly dissipated and weaker interactions dominated (Fig. 2c).

To probe experimentally the roles of K80, R45 and R269 in substrate binding, we mutated K80 to alanine, and R45 and R269 each to lysine, then tested the effects of these individual mutations on the transport activity and substrate-binding affinity of the protein. G3P was used as substrate in these biochemical experiments rather than P_i due to its higher binding affinity to GlpT[27] (see Materials and Methods). As expected, the wild type transporter reconstituted into proteoliposomes showed a clear uptake of substrate G3P, achieving a V_{max} of 487 nmol/min/mg (Fig. 2e and Table 1) — a value in accord with that published previously for wild type GlpT reconstituted into proteoliposomes.[28] None of the three mutants, however, retained transport activity (Fig. 2e), showing the critical importance of each of these residues for substrate transport in GlpT. These results mirror those of previous experiments performed on UhpT.[22] We then measured the substrate-binding affinity of these mutants in detergent solution by tryptophan fluorescence quenching. The R45K mutant showed no binding to substrate (Fig. 2f and Table 1), confirming the central role of this residue for transporter function. In contrast, both the K80A and R269K mutants retained some ability to bind G3P, although with apparent K_d's of 51 μM and 29 μM, respectively (Fig. 2f), which are about 98% and 97% less tight than wild-type GlpT binding to G3P (K_d of 0.8 μM).[19] We put forward, therefore, that tight substrate binding to GlpT, involving interaction with all the residues that form the substrate-binding site from both the N- and C-terminal domains, is required to drive the conformational changes necessary for transport. Mutation of either the K80 or the R269 residue loosens substrate binding and the intrinsic binding energy released by such weaker interaction is therefore insufficient to surmount the activation energy barrier of GlpT. Thus, conformational change and transport cannot be achieved.

Table 1. Transport kinetics and binding affinities to G3P of GlpT binding-site mutants

GlpT mutant	V_{max}* (nmol/min/mg)	K_m (μM)*	K_d (μM)**
WT	487±22	27±4	0.8±0.2
R45K	No transport	No transport	No binding
R269K	No transport	No transport	29±3.0
E299Q	46±3	64±12	4.5±0.3
H165P	30±2	52±10	62±6.0
K46L	52±5	124±27	3.9±0.7
D274N	163±17	177±39	1.1±0.2
K80A	No transport	No transport	51±5.2

* V_{max} and apparent K_m values were calculated from transport assays on GlpT reconstituted into proteoliposomes.
** Apparent K_d values were calculated from binding studies performed with GlpT in detergent solution.

The role of basic residues in binding oxyanionic substrates to GlpT reflects a common theme in biology: in enzymes that interact with P_i or organophosphates arginine and lysine residues are almost always involved in recognition of the anionic phosphoryl group.[29,30] In membrane transport of anions, such basic residues often form pairs that are essential for transport activity: Arg272 and Lys355 are involved in substrate binding to the oxalate:formate antiporter (OxlT) of *Oxalobacter formigenes*;[31] two arginine residues (R87 and R368) are functionally indispensable to the nitrate transporter, NtrA, from *Aspergillus nidulans*;[32] and R87 and R303 are essential to the putative *E. coli* nitrate:nitrite antiporter, NarU.[33]

Protonation of H165 allows tighter substrate binding

Another potentially important residue for substrate binding is H165, located at the apex of a triangle formed between it and the R45 and R269 residues (Fig. 1b). Little contact was established between histidine and the divalent P_i substrate during MD simulations where H165 was neutral (Fig. 2d). Strikingly, however, upon protonation of H165, strong participation in substrate coordination was observed in the simulation. A highly stable hydrogen bond of 1.5 Å was seen from the H165 δ–proton position to the P_i substrate (Fig. 3a).

Upon protonation of H165 in the simulation system, a reorientation within the substrate-binding pore of the substrate molecule itself was also observed, with it being localized closer towards the cytoplasmic end of the substrate-binding pore, and nearer to the C-terminal domain of the protein.

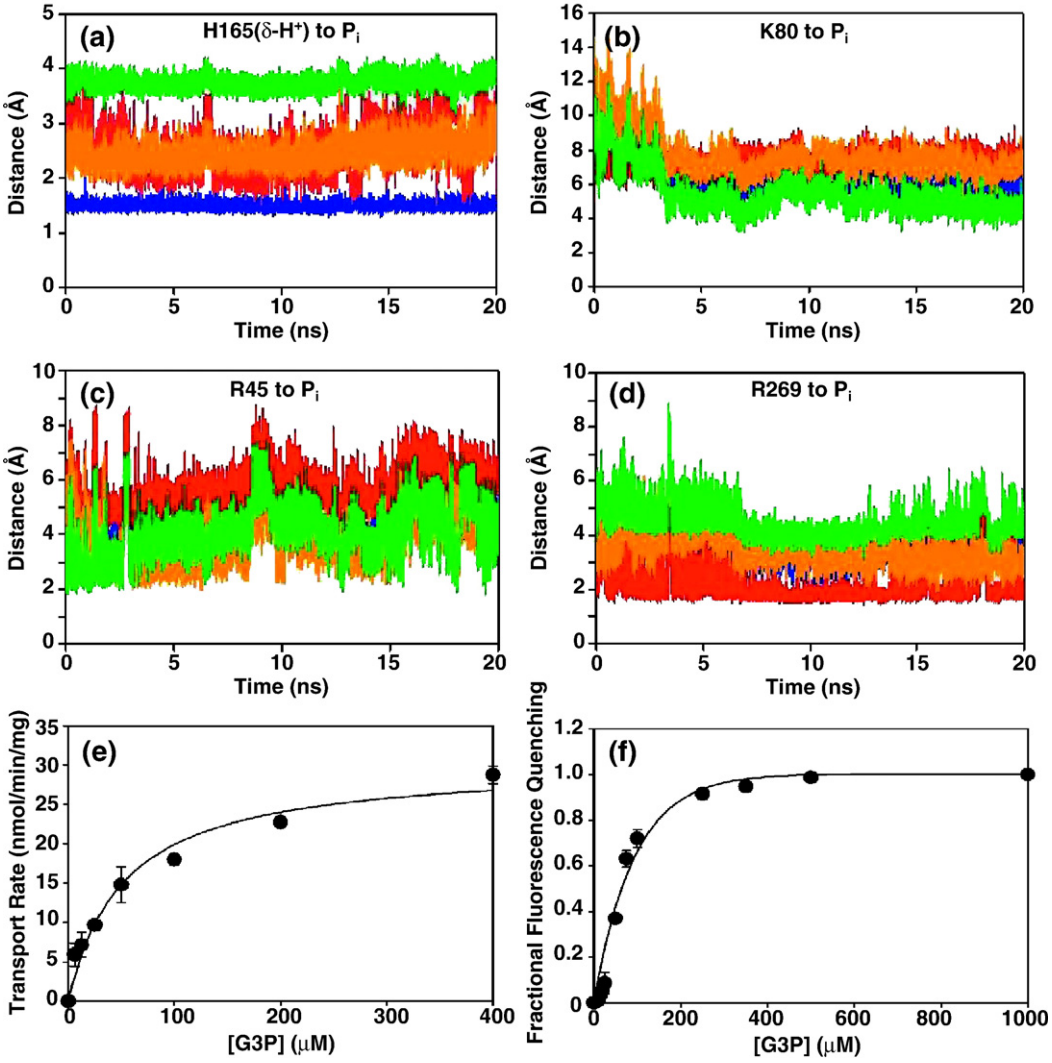

Fig. 3. Distances between the side chains of H165, K80, R45 and R269 of GlpT to the P_i substrate oxygens from molecular dynamics simulations of GlpT with P_i docked and H165 protonated (a–d); and experimental measurements of the effect of mutating H165 to proline on the transport activity and substrate-binding affinity of GlpT (E and F). Molecular dynamics simulations suggest that protonation of H165 induces tighter substrate binding to GlpT, along with a reorientation of the substrate molecule within the substrate-binding site. The distance from each side chain to the P_i oxygens is color-coded as follows: to O1, blue line; O2, red line; O3, orange line; and O4, green line. (a) distances from the δ–proton of H165 to P_i substrate. Protonated H165 interacts strongly with substrate, forming hydrogen bonds of 1.5–3 Å with three of the substrate oxygens; (b) K80 maintains a stable interaction with P_i upon protonation of H165; (c) there is a slight weakening of the interactions between R45 and the substrate oxygens when H165 is protonated; (d) protonation of H165 enables R269 to establish much stronger, more stable interactions of 2–4 Å with the substrate molecule; (e) transport activity assay of H165P GlpT reconstituted into proteoliposomes. The mutant displayed saturation kinetics but was less active than wt protein, with a V_{max} of 30 nmol/min/mg and a K_m of 52 μM; (f) substrate-binding affinity of the H165P mutant transporter to G3P measured in detergent solution. The mutant retained the ability to bind to substrate, although much less tightly than wt GlpT, with an apparent binding dissociation constant of 62 μM.

Protonation of H165 also caused K80 and R269 to bind more tightly to the substrate, whereas the substrate interaction with R45 was destabilized (Figs. 3b–d). A strong hydrogen bond of ~2.5 Å in length formed between R269 and P_i (Fig. 3d). Concomitantly, because of the movement of the substrate molecule closer to the C-terminal half of GlpT upon full protonation of H165, the interactions between R45 and P_i were weakened and fluctuating compared to those observed with unprotonated H165 (Fig. 2d). These results clearly suggested a role for H165, probably in a protonated form, in substrate binding. The source of the donated proton can only be speculated; it is most likely abstracted from one of the water molecules that fill the substrate-translocation pore of the transporter molecule.

We then investigated the role of the H165 residue in substrate binding by mutating it to a proline experimentally, followed by transport and binding assays. Although the H165P mutant folded properly, as judged by its having a similar retention time and peak shape as the wild type transporter in analytical size exclusion chromatography (data not shown), the mutation severely affects both transport and binding by GlpT (Table 1), the mutant having a V_{max} of 30 nmol/min/mg (Fig. 3e) and an apparent dissociation constant K_d of 62 μM (Fig. 3f). This represents about a 94% and 98% decrease in transport activity and substrate-binding affinity, respectively, compared to the wild type transporter (Table 1). However, the K_m of the H165P mutant (52 μM) showed less than 2-fold change compared to the wild-type protein (K_m of 27 μM). This emphasizes that caution must be exercised if K_m values derived from this type of experiment are interpreted simply as direct measures of binding affinity to these transporters.[34]

The fact that the proline side chain is not ionizable and is of similar bulk to histidine, indicates that loss of the protonation cycle in the H165P mutant is likely to be responsible for the impairment of both transport activity and substrate binding affinity, and by extension, that the protonation of H165 plays an important role in the transport reaction of GlpT. We could not directly test the role of histidine protonation in GlpT by altering the pH of our experimental systems, however, because this would also alter the ionization state of the P_i substrate itself (pK_{a2} of 7.2). While changes in histidine ionization state are common in many enzyme-catalyzed reactions,[35] several observations have highlighted its importance in membrane transporter proteins. In UhpT, protonation of the conserved histidine residue (H168), equivalent to H165 in GlpT, has been proposed to play a role in transport.[26] Similarly, single histidine residues have been shown to be important for proton or cation translocation in other MFS transporters such as *E. coli* LacY[36] and TetA,[37] and the rat vesicular monoamine transporter r-VMAT1,[38] as well as in members of other membrane transporter families.[39–43] In r-VMAT1, H419 is important for energy coupling.[38] In the plant tonoplast malate carrier, protonation of a histidine residue in the tentative substrate-binding site increases both affinity and transport rate.[39]

Another issue is the influence of local environment on histidine protonation. Is it possible for the histidine side chain, which has a pK_a of 6.02 in solution, to become protonated at the physiological pH (7.4) of the *E. coli* cytoplasm? The pK_a of histidine residues in proteins can be modulated by the local microenvironment and field effects.[44,45] In GlpT, the H165 residue is surrounded by several conserved aromatic residues (Y38, Y42, Y76, W138, W161, Y362 and Y393),[18] and histidine-aromatic interactions can contribute to elevation of histidine pK_a.[46–48] Therefore, we suggest the primary function of the conserved tyrosines and other surrounding aromatic residues of GlpT is not directly in substrate binding, but in stabilizing the basicity of the binding site. This would raise the pK_a of the histidyl residue enabling it to become protonated. Such a stabilizing role for tyrosine residues has been suggested for the mammalian H^+/peptide transporter, PepT1, a member of the proton-dependent oligopeptide transporter (POT) family which is also part of the MFS.[49]

Making and breaking of salt bridges controls the interconversion between the C_i and C_o conformations of GlpT

The crystal structure of GlpT[18] along with previous biochemical studies on UhpT[25] suggested three additional conserved, charged residues in the membrane-embedded region of GlpT–K46, D274 and E299 — to be of potential importance to transporter function (Fig. 1c). In fact, these three residues, along with K80, R45 and R269, are the only charged residues found within the hydrophobic core of GlpT which are all conserved. While K46, D274 and E299 do not directly bind substrate when GlpT is in the C_i state, as shown by MD simulations, they were found to play a key role in salt bridge formation (Fig. 4, Table 2). Their roles were tested in three separate simulation systems: (1) in the apoprotein in which H165 was unprotonated, a salt bridge of ~2 Å in length formed between D274 and K46, with a weaker, unstable salt bridge of ~4–6 Å formed between D274 and R45. No salt bridge formation was observed between E299 and R269 during the lifetime of the simulation, the distance between the side chains fluctuating between ~6–8 Å. However, a strong, stable salt bridge of 2.5 Å formed between E299 and K46 (Table 2); (2) with P_i docked to the unprotonated transporter, the D274–K46 interactions weakened and the distance between their side chains increased to between ~4–5 Å (Fig. 4a, black). Simultaneously, the attraction between D274 and R45 became much stronger, with a hydrogen bond of ~2 Å in length forming (Fig. 4b, black). Docking of P_i had little effect on the E299–K46 or E299–R269 interactions (Figs. 4c and d, respectively); (3) protonation of H165 caused the interaction between D274 and K46 to strengthen considerably, with a

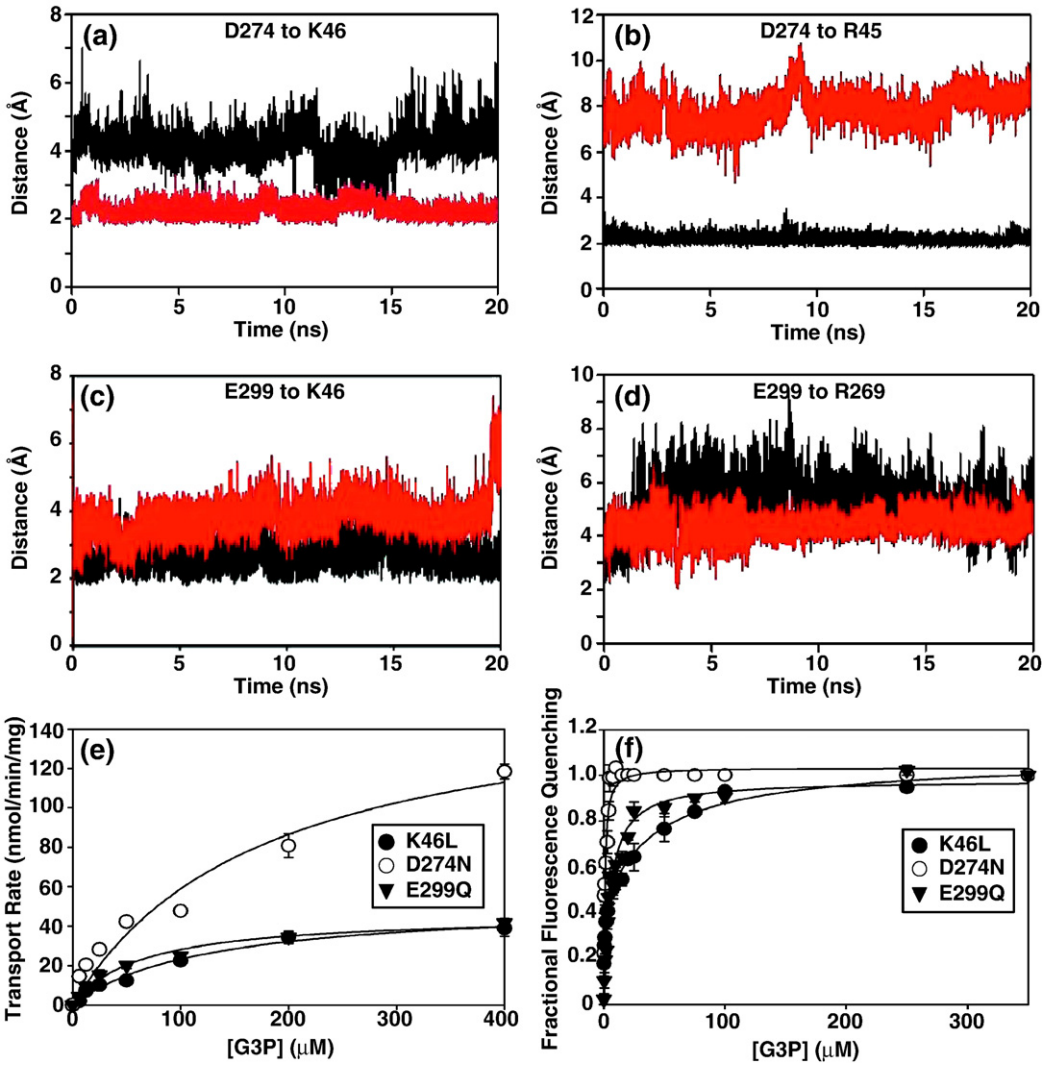

Fig. 4. The effect of protonating H165 upon distances between the side chains of residues that are proposed to participate in salt bridge formation, and experimental measurements of the effect of mutating those residues upon the transport activity and binding affinity of GlpT. (a) the distance between D274 and K46 when H165 is unprotonated (black line). Upon protonation of H165 these residues move closer to each other and form a strong interaction (red line); (b) a strong 2.5 Å interaction occurs between D274 and R45 when H165 is unprotonated (black line) that is disrupted upon protonation of H165 (red line); (c) there is a weakening of the interaction between E299 and K46 when H165 is protonated (red line) compared to when H165 is unprotonated (black line); (d) a stable intradomain salt bridge forms between E299 and R269 upon protonation of H165 (red line) that is much weaker and fluctuating when H165 is unprotonated (black line); (e) transport activity assay showing that the K46L, D274N and E299Q mutants all retain the ability to transport G3P substrate when reconstituted into proteoliposomes, but at much reduced rates compared to the wt protein. The K46L and E299Q mutants had similar V_{max} values of 52 and 46 nmol/min/mg, respectively. Their K_m values were 124 and 64 μM, respectively. The D274N mutation had the least deleterious effect on transport activity, the mutant having a V_{max} of 163 nmol/min/mg, and a K_m of 177 μM; (f) substrate-binding affinity assays performed on the K46L, D274N and E299Q mutant transporters in detergent solution. The K46L, D274N and E299Q mutants had K_d values of 3.9, 1.1 and 4.5 μM, compared to 0.8 μM for wt GlpT. The GlpT wt data are omitted for clarity. The assays suggested that these residues are not direct participants in substrate binding to GlpT, as all possessed calculated apparent K_d values similar to the wt protein.

minimum distance of about 2.5 Å (Fig. 4a, red). At the same time, the interaction between D274 and R45 dissolved completely (Fig. 4b, red) and the interaction between E299 and K46 weakened (Fig. 4c, red). The E299 and R269 side chains also moved closer together upon protonation of H165, forming a salt bridge of 4–5 Å in length (Fig. 4d, red).

Our transport activity and binding studies provided further evidence that although the K46, D274 and E299 residues are not directly involved in actual substrate binding to the transporter in the C_i conformation, they are still important for transport. For these experiments, K46 was mutated to leucine, D274 to asparagine and E299 to glutamine. All three mutants were found to possess apparent substrate-binding affinities comparable to the wild type protein (K46L K_d = 3.9 μM, D274N K_d = 1.1 μM, and E299Q K_d = 4.5 μM) (Fig. 4f and Table 1). However,

Table 2. Distances between residues involved in salt bridge formation in unprotonated GlpT apoprotein and during substrate-binding to GlpT when H165 is unprotonated and protonated

Ion Pair	Apoprotein, H165 unprotonated	P_i bound, H165 unprotonated	P_i bound, H165 protonated
D274–K46	~2 Å	4–5 Å	2.5 Å
D274–R45	4–6 Å	~2 Å	No salt bridge
E299–K46	2.5 Å	2.5 Å	3–4 Å
E299–R269	No salt bridge	No salt bridge	4–5 Å

mutation of either E299 to Q or K46 to L had a deleterious effect on the maximal transport activity of the protein, resulting in V_{max} values of 46 and 52 nmol/min/mg, respectively (Fig. 4e and Table 1), representing about a 90% decrease in the maximal transport rate measured for wild type protein. Mutation of the E299 and K46 residues also caused the K_m values to differ from that of the wild type protein, with the E299Q transporter having a K_m of 46 μM, whereas the K46L transporter had a K_m of 124 μM (Table 1), yielding about a 2-fold and 4-fold increase compared to wild type protein, respectively. Mutation of the D274 residue to asparagine resulted in the V_{max} decreasing by 66% compared to wild type, to 163 nmol/min/mg (Table 1). This D274N mutation, however, had a bigger effect on K_m, the value of which — 177 μM–represents over a 6-fold increase compared to that of wild type GlpT. Therefore, it is clear that the major effect of mutating the E299, K46 and D274 residues is on the turnover of the transporter, rather than on binding affinity. Combining our MD simulation and biochemical results, we hypothesize that the interdomain salt bridges formed by D274 with K46 and R45, and by E299 with K46, act in concert to control the relative motions of the two domains of GlpT during the transport reaction cycle. We were unable to test the effects of the salt bridge formation and breaking on GlpT using MD simulations however, because the complete cycle of transport occurs during milliseconds,[27] a timescale that is currently out of reach for this technique.

Proposed mechanism for substrate-induced conformational change

In this study, we addressed the substrate-binding mechanism of GlpT. Previous studies on UhpT, a close homologue of GlpT, had shown that the rate-limiting step of the transport cycle is the interconversion of the substrate-binding site; substrate-binding itself is rapid.[50] Integrating data from computational and biochemical studies on GlpT in a coherent manner has allowed us to propose a mechanism for substrate binding to the inward-facing C_i conformation of the transporter. The proposed substrate-binding mechanism consists of three stages: (1) initially, in the unloaded transporter, weak interactions exist between D274 and R45, and E299 and R269. At the same time, however, there are strong salt bridges formed between D274 and K46, and E299 and K46. Substrate then binds weakly to K80, R45 and R269 at the inner end of the substrate-binding pore. At this stage, H165 is unprotonated and does not participate strongly in binding. Substrate binding weakens D274's interaction with K46, and strengthens its interaction with another charged residue, R45, instead (Fig. 5a); (2) H165 then undergoes protonation, probably facilitated by the proximity of P_i, and its side chain moves much closer toward and interacts more strongly with the substrate. Coupled with a reorientation of

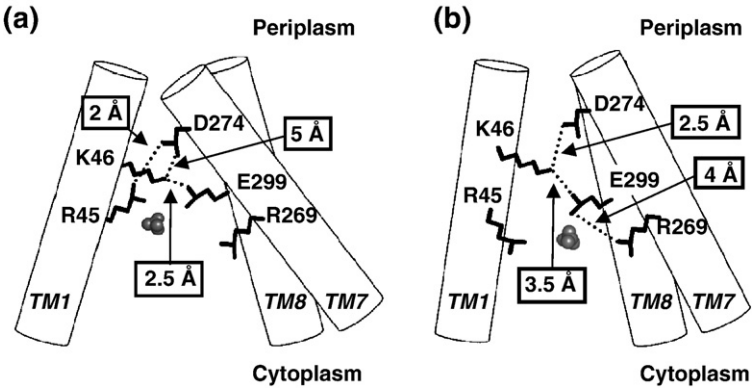

Fig. 5. Schematic diagram illustrating the inter- and intradomain salt bridge formation and breakage that occurs upon substrate binding and subsequent protonation of H165, and that is proposed to control conformational change of GlpT. (a) initially, when P_i binds weakly to GlpT, and H165 is unprotonated, strong interdomain salt bridges of ~2 and 2.5 Å exist between D274 and R45, and E299 and K46, respectively. A weaker interdomain salt bridge of ~5 Å is formed between D274 and K46; (b) protonation of H165 causes substrate to bind more tightly and disrupts the D274–R45 interdomain salt bridge, and weakens the E299-K46 one. In contrast the D274–K46 interdomain salt bridge becomes much stronger, with a distance between side chains of 2.5 Å, and an intradomain salt bridge is formed between E299 and R269. This pulls the domains together and results in a more compact structure of the transporter. Transmembrane helices 1, 7 and 8 are represented as cylinders, the amino acid side chains that participate in salt bridge formation as black sticks, and salt bridges as dotted lines. The P_i substrate is represented as grey van der Waals spheres.

the substrate molecule, this elicits tighter overall binding to the transporter. Disruption of the interdomain D274–R45 salt bridge, and the weakening of the E299–K46 one, accompanied by the formation of stronger inter- and intradomain ones between D274 and K46, and E299 and R269, respectively, which occurs upon protonation of H165, is triggered by the pulling together of helices 1 and 7 by the R45 and R269 residues upon tight substrate binding (Fig. 5b). This results in an interdomain movement and relative rotation of the helices in each domain; (3) subsequent deprotonation of H165 would then weaken the interactions with the substrate allowing it to be released into the periplasm.

This proposed mechanism is consistent with previous theoretical considerations for membrane transporter systems that reduction in the energy barrier to conformational change — paid for by intrinsic binding energy between substrate and its binding site — is dependent on formation of an initial loose complex, followed by a tight complex in the transition state.[20] In our proposal, the salt bridge dynamics are part of the molecular "spring" that permits the delicately poised GlpT molecule to flip — via the rocker-switch mechanism[17,18] — from the substrate-bound inward-facing C_i–S conformation to the outward-facing C_o–S conformation. The salt bridges may even act as the "pivot" upon which the "teeter-totter" or "see-saw" motion of the two domains of the protein is centered. Such a mechanism is probably conserved amongst OPA family transporters. It is pertinent to note here that salt bridge formation and disruption upon substrate binding has been proposed previously to play a role in substrate translocation by the *E. coli* MFS symporter LacY.[51]

Materials and Methods

Simulation systems for molecular dynamics

Three sets of simulation conditions were used (designated systems 1–3). The initial simulation system (system 1) investigated the GlpT apoprotein and consisted of residues His10 to Glu448 of GlpT (Protein Data Bank accession code 1PW4), 444 POPE molecules, 24522 water molecules and 3 chlorine ions. This system was prepared by manually inserting the protein in the x–y plane of a previously simulated POPE bilayer,[52] upon which excess phospholipid molecules were removed and water molecules as well as chlorine ions were added to electroneutralize the system. The final system dimensions measured $121 \times 121 \times 92$ Å after constant number of particles, pressure and temperature (NPT) equilibration (see below). The other two simulation conditions differed from the apoprotein system only in that a divalent P_i substrate was added to one (system 2), and both a divalent P_i was added and H165 was protonated in the other (system 3). In addition, two chloride ions were removed from system 2 and one chloride ion was removed from system 3 in order to maintain electroneutrality. The divalent P_i molecule was docked to the substrate-translocation pore by AUTODOCK3[53] using standard grid spacing and 1000 searches with the Lamarckian Genetic Algorithm. P_i charges were obtained from the PRODRG server.[54] Finally, three control systems were generated, differing only from systems 2 and 3 in that ESP/RESP derived charges[55] were used for the electrostatic model of the divalent P_i molecule.

Molecular dynamics simulations

Molecular dynamics simulations were carried out with GROMACS version 3.3.1[56,57] using an integration time step of 1 fs. The short time step was used to avoid strong steric fluctuations inside the pore. A modified version of the GROMOS87 force field was used for the protein and complemented with the OPLS/Berger force field for the lipids.[58] Lipid topology files were obtained from Peter Tieleman's web site (http://moose.bio.ucalgary.ca/). The SPC water model was used.[59] Upon assembly, System 1 underwent energy minimization using the steepest descent algorithm (Fmax <2000 kJ mol^{-1} nm^{-1}, <100 steps) followed by 2 ns of position restrained NPT simulation where the protein coordinates were restrained. Systems 2 and 3 (derived from system 1 at this point, see above) underwent additional energy minimization (Fmax <2000 kJ mol^{-1} nm^{-1}, <40 steps) prior to 20 ns unrestrained NPT simulation of all systems. Ewald summation was employed using a Particle Mesh Ewald method.[60] The bond lengths were constrained with the LINCS algorithm[61] and the SETTLE algorithm was used to make the water molecules rigid.[62] Temperature was maintained constant by separately coupling protein, lipids, water and P_i to a Berendsen heat bath[63] at 310 K, using a time constant $\tau_T = 0.1$ ps. An isotropic external pressure of 1 atmosphere was maintained using pressure coupling with a compressibility constant $\kappa = 4.5 \times 10^{-5}$ bar^{-1} and a time constant $\tau_P = 1.0$ ps.

Bacterial strains, plasmids and site-directed mutagenesis

All GlpT protein used in this study was expressed in phage-resistant *E. coli* LMG194 cells using the pBAD/*Myc*-HisA expression vector system (Invitrogen, Carlsbad, CA). The GlpT construct used consisted of amino acids 1–448 followed by a C-terminal thrombin-specific cleavage site, *myc*-epitope and His6-tag (pBAD-GlpT-Thr-*Myc*-His A) as described before.[27] Site-directed mutagenesis for the E299Q, H165P, K46L and D274N mutants was performed using the conventional oligonucleotide-mediated double primer method with pBAD-GlpT-Thr-*Myc*-His A as a template. The R45K, R269K and K80A mutant GlpT transporters were constructed using the QuikChange site-directed mutagenesis kit (Stratagene, Cedar Creek, TX). Mutations were confirmed by sequence analysis of the full-length plasmid DNA.

Cell culture, protein purification and reconstitution of GlpT

Cells were cultured and protein used for substrate binding affinity assays was purified to homogeneity as described previously.[27] The yield of GlpT mutants was found to be comparable to that of wild-type. The protocol for purification of His-tagged GlpT for reconstitution into proteoliposomes has been published before.[19] Reconstitution of GlpT into proteoliposomes was performed using a detergent dilution method based on that described previously.[28] Initially, unilamellar vesicles were prepared

by adding 1 mL of ice-cold loading buffer (100 mM KP_i at pH 7.0) to 10 mg of *E. coli* polar lipid extract (Avanti Polar Lipids, Alabaster, AL), vortexed vigorously then sonicated on ice until the lipid was dissolved. 1.5% (w/v) *n*–octyl-β-D-glucopyranoside (β-OG) (Anatrace, Maumee, OH) was then added to the mixture to destabilize the liposomes, along with 10 μg of nickel-nitriloacetic acid (Ni-NTA)-purified His-tagged GlpT to give a lipid:protein ratio of 1000:1. This was followed by 20 minutes stirring on ice to allow the protein to insert. Proteoliposomes were formed by a 20-fold dilution with room temperature loading buffer. After harvesting by centrifugation at 180 000***g*** for 1 h, the surface of the proteoliposome pellet was washed twice with ice-cold assay buffer (100 mM K_2SO_4, 50 mM MOPS-K at pH 7.0) prior to the proteoliposomes being taken up in 1 mL of the same buffer. Proteoliposomes were used immediately for transport assays. For control experiments, the above protocol was used to prepare liposomes to which only Ni-NTA elution buffer, not protein, was added.

Transport assays

Transport assays of mutant GlpT transporters reconstituted into liposomes preloaded with saturating concentrations of KP_i allowed quantitation of the heterologous G3P-P_i antiport reaction by measuring the uptake of radiolabeled G3P. Freshly prepared proteoliposomes were taken up in 250 μL of assay buffer and 5 μL of these were diluted 10-fold with the same buffer. The proteoliposomes were equilibrated to 37 °C for 1 min prior to addition of [^{14}C]-G3P (150 mCi/mmol) (American Radiolabeled Chemicals, St. Louis, MO) covering a range of concentrations from 6.25 μM to 400 μM. The reaction was allowed to proceed for 1 min before 50 μL of proteoliposomes were removed and applied to 0.22 μm nitrocellulose filters (Millipore GSWP 02500) mounted on a Hoeffer vacuum manifold. The transport reaction was terminated by washing the filter-bound proteoliposomes with two 5 mL aliquots of ice-cold assay buffer. The filters were incubated overnight in liquid scintillant (ScintiLene, Fisher Scientific) prior to measuring the radioactivity incorporated into the proteoliposomes using a Wallac 1450 Microbeta Plus liquid scintillation counter. After subtraction of the radioactivity associated with control liposomes at each concentration of substrate studied, the radioactive counts per minute of experiments performed in triplicate were converted into values of nmols of substrate transported per min per mg GlpT. To guarantee reproducibility of the method, transport assays using wild-type GlpT were performed along with each mutant transporter as well as control experiments using liposomes to which no protein, only buffer, had been added. The latter was to ensure that incorporation of radiolabeled substrate was due only to activity of the transporter and not uptake through a leaky proteoliposome. The resultant data were used to determine the apparent kinetic constants (K_m and V_{max}) for G3P uptake as described in the past.[19]

Substrate binding affinity assays

Affinity of both wild-type and mutant GlpT to G3P was assayed by measuring the quenching of the intrinsic tryptophan fluorescence of GlpT upon binding of substrate in detergent solution as described previously.[19,27] G3P was chosen as a substrate over P_i due to its higher affinity to GlpT. Briefly, measurements were performed on a Fluoromax-2 fluorimeter (Jobin-Yvon, Edison, NJ) with excitation and emission wavelengths of 283 nm and 334 nm, respectively, and a protein concentration of 0.01 mg/mL. The GlpT protein used for binding studies was purified to homogeneity using size-exclusion chromatography as described by Auer et al.[27] The protein solution was titrated with *sn*-glycerol 3-phosphate bis(cyclohexylammonium) salt (Sigma, St. Louis, MO) until full fluorescence quenching was observed (typically 0.25 μM–1000 μM). After subtraction of the buffer blank and correction for dilution, the fractional fluorescence quenching was plotted as a function of G3P substrate concentration. The data then underwent nonlinear regression analysis as described earlier[19] to enable calculation of apparent dissociation constant values. Experiments were performed in triplicate at a temperature of 37 °C. It should be noted that the apparent K_d values reported here are approximate, as the steady state substrate-binding affinity measurements were performed on the purified transporter in detergent solution. Under these conditions, DDM binds to the substrate-binding pore and has to be competed off by the G3P substrate before the affinity of G3P to GlpT can be measured.

Acknowledgements

The authors would like to thank Dr. Greg Boel, Columbia University, New York for the gift of phage-resistant *E. coli* LMG194 cells, Regina Fong for assistance in constructing the GlpT mutants, Kelly Molloy for stability measurements of the mutants, and Dr. Nathan Karpowich for critical reading of the manuscript. J.A. and A.L. thank the Swedish National Infrastructure for Computing (SNIC) for allocation of computing time. A.L. thanks the Swedish Science Council (VR) for financial support. This work was supported in part by NIH grant DK-053973 (to D.N.W.).

References

1. Hayashi, S., Koch, J. P. & Lin, E. C. C. (1964). Active transport of L-α-glycerophosphate in *Escherichia coli*. *J. Biol. Chem.* **239**, 3098–3105.
2. Lin, E. C. C. (1976). Glycerol dissimilation and its regulation in bacteria. *Ann. Rev. Microbiol.* **30**, 535–578.
3. Rao, N. N., Roberts, M. F., Torriani, A. & Yashphe, J. (1993). Effect of glpT and glpD mutations on expression of the phoA gene in *Escherichia coli*. *J. Bacteriol.* **175**, 74–79.
4. Andersson, S. G., Zomorodipour, A., Andersson, J. O., Sicheritz-Ponten, T., Alsmark, U. C., Podowski, R. M. *et al.* (1998). The genome sequence of *Rickettsia prowazekii* and the origin of mitochondria. *Nature*, **396**, 133–140.
5. Nilsson, R. P., Beijer, L. & Rutberg, B. (1994). The glpT and glpQ genes of the glycerol regulon in *Bacillus subtilis*. *Microbiology*, **140**, 723–730.
6. Song, X. M., Forsgren, A. & Janson, H. (1998). Glycerol-3-phosphate transport in *Haemophilus influenzae*: cloning, sequencing, and transcription analysis of the glpT gene. *Gene*, **215**, 381–388.
7. Venkatesan, M. M., Alexander, W. A. & Fernandez-Prada, C. (1996). A *Shigella flexneri* invasion plasmid

gene, ipgH, with homology to IS629 and sequences encoding bacterial sugar phosphate transport proteins. *Gene*, **175**, 23–27.
8. Bevan, M., Bancroft, I., Bent, E., Goodman, H., Dean, C., Bergkamp, R. *et al.* (1998). Analysis of 1.9 Mb of contiguous sequence from chromosome 4 of *Arabidopsis thaliana*. *Nature*, **391**, 485–488.
9. Bartoloni, L., Wattenhofer, M., Kudoh, J., Berry, A., Shibuya, K., Kawasaki, K. *et al.* (2000). Cloning and characterization of a putative human glycerol 3-phosphate permease gene (SLC37A1 or G3PP) on 21q22.3: Mutation analysis in two candidate phenotypes. DFNB10 and a glycerol kinase deficiency. *Genomics*, **70**, 190–200.
10. Pao, S. S., Paulsen, I. T. & Saier, M. H. (1998). Major facilitator superfamily. *Microbiol. Mol. Biol. Rev.* **62**, 1–34.
11. Maloney, P. C., Ambudkar, S. V., Anatharam, V., Sonna, L. A. & Varadhachary, A. (1990). Anion-exchange mechanisms in bacteria. *Microbiol. Rev.* **54**, 1–17.
12. Sa-Correia, I. & Tenreiro, S. (2002). The multidrug resistance transporters of the major facilitator superfamily, 6 years after disclosure of *Saccharomyces cerevisiae* genome sequence. *J. Biotechnol.* **98**, 215–226.
13. Saier, M. H., Jr., Beatty, J. T., Goffeau, A., Harley, K. T., Heijne, W. H., Huang, S. C., Jack, D. L. *et al.* (1999). The major facilitator superfamily. *J. Mol. Microbiol. Biotech.* **1**, 257–279.
14. Abramson, J., Smirnova, I., Kasho, V., Verner, G., Kaback, H. R. & Iwata, S. (2003). Structure and mechanism of the lactose permease of *Escherichia coli*. *Science*, **301**, 610–615.
15. Kaback, H. R. (1997). A molecular mechanism for energy coupling in a membrane transport protein, the lactose permease of *Escherichia coli*. *Proc. Natl. Acad. Sci. USA*, **94**, 5539–5543.
16. Vidavar, G. A. (1966). Inhibition of parallel flux and augmentation of counter flux shown by transport models not involving a mobile carrier. *J. Theor. Biol.* **10**, 301–306.
17. Lemieux, M. J., Huang, Y. & Wang, D. N. (2004). Structural basis of substrate translocation by the *Escherichia coli* glycerol-3-phosphate transporter: a member of the major facilitator superfamily. *Curr. Opin. Struct. Biol.* **14**, 405–412.
18. Huang, Y., Lemieux, M. J., Song, J., Auer, M. & Wang, D. N. (2003). Structure and mechanism of the glycerol-3-phosphate transporter from *Escherichia coli*. *Science*, **301**, 616–620.
19. Law, C. J., Yang, Q., Soudant, C., Maloney, P. C. & Wang, D. N. (2007). Kinetic evidence is consistent with the rocker-switch mechanism of membrane transport by GlpT. *Biochemistry*, **46**, 12190–12197.
20. Krupka, R. M. (1989). Role of substrate binding forces in exchange-only transport systems: I. Transition-state theory. *J. Membr. Biol.* **109**, 151–158.
21. Krupka, R. M. (1989). Role of substrate binding forces in exchange-only transport systems: II. Implications for the mechanism of the anion exchanger of red cells. *J. Membr. Biol.* **109**, 159–171.
22. Fann, M. C., Davies, A. H., Varadhachary, A., Kuroda, T., Sevier, C., Tsuchiya, T. & Maloney, P. C. (1998). Identification of two essential arginine residues in UhpT, the sugar phosphate antiporter of *Escherichia coli*. *J. Membr. Biol.* **164**, 187–195.
23. Almqvist, J., Huang, Y., Hovmöller, S. & Wang, D. N. (2004). Homology modeling of the human microsomal glucose-6-phosphate transporter explains the mutations that cause the glycogen storage disease type Ib. *Biochemistry*, **43**, 9289–9297.
24. Chen, L. Y., Pan, C. J., Shieh, J. J. & Chou, J. Y. (2002). Structure-function analysis of the glucose-6-phosphate transporter deficient in glycogen storage disease type Ib. *Hum. Mol. Genet.* **11**, 3199–3207.
25. Hall, J. A., Fann, M. C. & Maloney, P. C. (1999). Altered substrate selectivity in a mutant of an intrahelical salt bridge in UhpT, the sugar phosphate carrier of *Escherichia coli*. *J. Biol. Chem.* **274**, 6148–6153.
26. Hall, J. A. & Maloney, P. C. (2005). Altered oxyanion selectivity in mutants of UhpT, the P_i-linked sugar phosphate carrier of *Escherichia coli*. *J. Biol. Chem.* **280**, 3376–3381.
27. Auer, M., Kim, M. J., Lemieux, M. J., Villa, A., Song, J., Li, X. D. & Wang, D. N. (2001). High-yield expression and functional analysis of *Escherichia coli* glycerol-3-phosphate transporter. *Biochemistry*, **40**, 6628–6635.
28. Fann, M. C., Busch, A. & Maloney, P. C. (2003). Functional characterization of cysteine residues in GlpT, the glycerol 3-phosphate transporter of *Escherichia coli*. *J. Bacteriol.* **185**, 3863–3870.
29. Riordan, J. F. (1979). Arginyl residues and anion binding sites in proteins. *Mol. Cell. Biochem.* **26**, 71–92.
30. Skarzynski, T., Mistry, A., Wonacott, A., Hutchinson, S. E., Kelly, V. A. & Duncan, K. (1996). Structure of UDP-N-acetylglucosamine enolpyruvyl transferase, an enzyme essential for the synthesis of bacterial peptidoglycan, complexed with substrate UDP-N-acetylglucosamine and the drug fosfomycin. *Structure*, **4**, 1465–1474.
31. Wang, X., Sarker, R. I. & Maloney, P. C. (2006). Analysis of substrate-binding elements in OxlT, the oxalate:formate antiporter of *Oxalobacter formigenes*. *Biochemistry*, **45**, 10344–10350.
32. Unkles, S. E., Rouch, D. A., Wang, Y., Siddiqi, M. Y., Glass, A. D. & Kinghorn, J. R. (2004). Two perfectly conserved arginine residues are required for substrate binding in a high-affinity nitrate transporter. *Proc. Natl. Acad. Sci. USA*, **101**, 17549–17554.
33. Jia, W. & Cole, J. A. (2005). Nitrate and nitrite transport in *Escherichia coli*. *Biochem. Soc. Trans.* **33**, 159–161.
34. Van Winkle, L. J. (1995). Transport kinetics. pp. 90–91, Academic Press, New York.
35. Schneider, F. (1978). Histidine in enzyme active centers. *Angew. Chem. Int. Ed. Engl.* **17**, 583–592.
36. Padan, E., Sarkar, H. K., Viitanen, P. V., Poonian, M. S. & Kaback, H. R. (1985). Site-specific mutagenesis of histidine residues in the lac permease of *Escherichia coli*. *Proc. Natl. Acad. Sci. USA*, **82**, 6765–6768.
37. Yamaguchi, A., Samejima, T., Kimura, T. & Sawai, T. (1996). His257 is a uniquely important histidine residue for tetracycline/H^+ antiport function but not mandatory for full activity of the transposon Tn10-encoded metal-tetracycline/H^+ antiporter. *Biochemistry*, **35**, 4359–4364.
38. Shirvan, A., Laskar, O., Steiner-Mordoch, S. & Schuldiner, S. (1994). Histidine-419 plays a role in energy coupling in the vesicular monoamine transporter from rat. *FEBS Lett.* **356**, 145–150.
39. Dietz, K. J., Canut, H. & Marigo, G. (1992). Identification of an essential histidine residue at the active site of the tonoplast malate carrier in *Catharanthus roseus* cells. *J. Membr. Biol.* **129**, 137–143.
40. Dibrov, P., Young, P. G. & Fliegel, L. (1998). Functional analysis of amino acid residues essential for activity in the Na^+/H^+ exchanger of fission yeast. *Biochemistry*, **37**, 8282–8288.
41. Gerchman, Y., Olami, Y., Rimon, A., Taglicht, D., Schuldiner, S. & Padan, E. (1993). Histidine-226 is part

of the pH sensor of NhaA, a Na^+/H^+ antiporter in *Escherichia coli*. *Proc. Natl. Acad. Sci. USA*, **90**, 1212–1216.
42. Poolman, B., Modderman, R. & Reizer, J. (1992). Lactose transport system of *Streptococcus thermophilus*. The role of histidine residues. *J. Biol. Chem.* **267**, 9150–9157.
43. Pourcher, T., Sarkar, H. K., Bassilana, M., Kaback, H. R. & Leblanc, G. (1990). Histidine-94 is the only important histidine residue in the melibiose permease of *Escherichia coli*. *Proc. Natl. Acad. Sci. USA*, **87**, 468–472.
44. Coster, H. G. & Chilcott, T. C. (2002). Electric field effects in proteins in membranes. *Bioelectrochemistry*, **56**, 141–146.
45. Cymes, G. D., Ni, Y. & Grosman, C. (2005). Probing ion-channel pores one proton at a time. *Nature*, **438**, 975–980.
46. Dougherty, D. A. (1996). Cation-π interactions in chemistry and biology: a new view of benzene, Phe, Tyr, and Trp. *Science*, **271**, 163–168.
47. Loewenthal, R., Sancho, J. & Fersht, A. R. (1992). Histidine-aromatic interactions in barnase. Elevation of histidine pKa and contribution to protein stability. *J. Mol. Biol.* **224**, 759–770.
48. Tishmack, P. A., Bashford, D., Harms, E. & Van Etten, R. L. (1997). Use of ^{1}H NMR spectroscopy and computer simulations To analyze histidine pKa changes in a protein tyrosine phosphatase: experimental and theoretical determination of electrostatic properties in a small protein. *Biochemistry*, **36**, 11984–11994.
49. Chen, X. Z., Steel, A. & Hediger, M. (2000). Functional roles of histidine and tyrosine residues in the H^+-peptide transporter PepT1. *Biochem. Biophys. Res. Comm.* **272**, 726–730.
50. Fann, M. C. & Maloney, P. C. (1998). The functional symmetry of UhpT, the sugar phosphate transporter of *Escherichia coli*. *J. Biol. Chem.* **273**, 33735–33740.
51. Mirza, O., Guan, L., Verner, G., Iwata, S. & Kaback, H. R. (2006). Structural evidence for induced fit and a mechanism for sugar/H^+ symport in LacY. *EMBO J.* **25**, 1177–1183.
52. Tieleman, D. P., Forrest, L. R., Sansom, M. S. & Berendsen, H. J. (1998). Lipid properties and the orientation of aromatic residues in OmpF, influenza M2, and alamethicin systems: molecular dynamics simulations. *Biochemistry*, **37**, 17554–17561.
53. Morris, G. M., Goodsell, D. S., Halliday, R. S., Huey, R., Hart, W. E., Belew, R. K. & Olson, A. J. (1998). Automated docking using a Lamarckian genetic algorithm and empirical binding free energy function. *J. Comp. Chem.* **19**, 1639–1662.
54. Schuttelkopf, A. W. & Van Aalten, D. M. (2004). PRODRG: a tool for high-throughput crystallography of protein-ligand complexes. *Acta. Cryst. D*, **60**, 1355–1363.
55. Dupradeau, F. Y., Cezard, C., Lelong, R., Stanislawiak, E., Pecher, J., Delepine, J. C. & Cieplak, P. (2008). R.E. DD.B.: A database for RESP and ESP atomic charges, and force field libraries. *Nucleic Acids Res.* **36**, D360–D367.
56. Berendsen, H. J. C., Van der Spoel, D. & Van Drunen, R. (1995). Gromacs - a message-passing parallel molecular dynamics implementation. *Comp. Phys. Comm.* **91**, 43–56.
57. Lindahl, E., Hess, B. & Van der Spoel, D. (2001). GROMACS 3.0: a package for molecular simulation and trajectory analysis. *J. Mol. Mod.* **7**, 306–317.
58. Berger, O., Edholm, O. & Jahnig, F. (1997). Molecular dynamics simulations of a fluid bilayer of dipalmitoylphosphatidylcholine at full hydration, constant pressure, and constant temperature. *Biophys. J.* **72**, 2002–2013.
59. Berendsen, H. J. C., Postma, J. P. M., Van Gunsteren, W. F. & Hermans, J. (1981). Interaction models for water in relation to protein hydration. In Intermolecular Forces (Pullman, B., ed), pp. 331–342, D. Reidel Publishing Company, Dordrecht.
60. Essman, U., Perera, L., Berkowitz, M., Darden, T., Lee, H. & Pedersen, L. (1995). A smooth particle mesh Ewald method. *J. Chem. Phys.* **103**, 8577–8593.
61. Hess, B., Bekker, H., Berendsen, H. J. C. & Fraaije, J. G. E. M. (1997). LINCS: A linear constraint solver for molecular simulations. *J. Comp. Chem.* **18**, 1463–1472.
62. Miyamoto, S. & Kollman, P. A. (1992). Settle — an analytical version of the shake and rattle algorithm for rigid water models. *J. Comp. Chem.* **13**, 952–962.
63. Berendsen, H. J. C., Postma, J. P. M., Van Gunsteren, W. F., DiNola, A. & Haak, J. R. (1984). Molecular dynamics with coupling to an external bath. *J. Chem. Phys.* **81**, 3684–3690.